



Contents lists available at ScienceDirect

LWT

journal homepage: [www.elsevier.com/locate/lwt](http://www.elsevier.com/locate/lwt)

# Printable embedded pattern designs affect mechanical performance of cold-water fish gelatin cast films

Hongbo Sun<sup>a,b,c</sup>, Xiaojing Leng<sup>c</sup>, Xiaonan Sui<sup>b</sup>, Lu Zhang<sup>a,\*\*</sup>, Patrick Wilms<sup>a,\*</sup>

<sup>a</sup> Laboratory of Food Process Engineering, Wageningen University and Research, P.O. Box 17, 6700 AA, Wageningen, the Netherlands

<sup>b</sup> College of Food Science, Northeast Agricultural University, Harbin, 150030, China

<sup>c</sup> Key Laboratory of Functional Dairy, College of Food Science and Nutritional Engineering, China Agricultural University, Beijing, 100083, China

## ARTICLE INFO

### Keywords:

Edible film  
Tensile strength  
Stretching directions  
3D-printing  
Anisotropy

## ABSTRACT

Edible films made of cold-water fish gelatin suffer from suboptimal mechanical strength, limiting their use for sustainable packaging applications. In this study, the use of 3D-printable embedded patterns is investigated as reinforcement for gelatin cast films, aiming for cast films with customizable and enhanced mechanical strength. Various combinations of patterns (i.e. lines, grids, and triangles) and inks (varying concentrations of sodium caseinate, sodium alginate, and cellulose fibers) were 3D-printed. The 3D-printed structures were embedded into cast films and the mechanical properties were subsequently tested. Our results show that films with embedded patterns had an overall higher tensile strength at different stretching directions (i.e. parallel, perpendicular, and diagonal), compared to the plain gelatin films. The strongest mechanical anisotropy was found using the line pattern and the grid showed anisotropy in the parallel and perpendicular direction, highlighting the influence of printing path. Microscopical analysis revealed that embedded patterns affected the fracture mechanics of films. Interestingly, cellulose fibers showed alignment in the printed filaments along the printing direction, which contributes to an increased tensile strength of films after drying. Thus, by using printable embedded pattern design, edible films with customized mechanical performance can be made, contributing to future developments of sustainable packaging solutions.

## 1. Introduction

Plastics are common packaging materials for food products, which are nonbiodegradable and nonedible. Plastic food packages can lead to environmental pollution when discarded irresponsibly and cause health problems due to their direct contact with food (Groh et al., 2019; Ong, Samsudin, & Soto-Valdez, 2022). There is a growing consumer demand for high quality packaging materials, ready-to-eat food and reduction of ecological contaminations. Hence, edible biopolymers are increasingly used in commercial food products as sustainable packaging materials (Mohamed, El-Sakhawy, & El-Sakhawy, 2020). Numerous natural biopolymers such as polysaccharides, proteins and lipids are developed into edible coating or films as food packaging (Ghosh, Ziegler, & Anantheswaran, 2005; Hernández, Emaldi, & Tovar, 2008; Mohamed et al., 2020). Food packages made of these materials can protect food products from damages, preserve flavor and nutritional value during storage, handling, and transportation. They can in principle be eaten by

consumers without any adverse effect on health.

Gelatin as a biocompatible material has gained abundant attention for food packaging, bioengineering, and wound treatment applications due to its excellent film forming ability, biodegradability, and edibility (Yang, Chaieb, & Hemar, 2021). Cold-water fish gelatin is a by-product in fish processing, which acts as an alternative to mammalian gelatins (Zhang, Versteeg, Alting, & Schutyser, 2020). However, fish gelatin films suffer from poor tensile strength, limiting their applications as a sustainable packaging material (Hanani, Yee, & Nor-Khaizura, 2019; Hosseini, Javidi, & Rezaei, 2016). In previous research, additives incorporated into fish gelatin films were shown to enhance their mechanical performance (Chen et al., 2022; Li et al., 2024). Although blending additives in fish gelatin can effectively influence the performance of the obtained films, it does not allow for easy customization for specific applications. Customized edible packaging could provide solutions to designs that require structural strengthening (e.g. handle of a bag) or even directional tearing (e.g. easy tearing notches). Thus,

\* Corresponding author.

\*\* Corresponding author.

E-mail addresses: [lu1.zhang@wur.nl](mailto:lu1.zhang@wur.nl) (L. Zhang), [patrick.wilms@wur.nl](mailto:patrick.wilms@wur.nl) (P. Wilms).

<https://doi.org/10.1016/j.lwt.2024.116839>

Received 18 June 2024; Received in revised form 5 September 2024; Accepted 27 September 2024

Available online 28 September 2024

0023-6438/© 2024 The Authors. Published by Elsevier Ltd. This is an open access article under the CC BY license (<http://creativecommons.org/licenses/by/4.0/>).

instead of using a homogenous mixture, embedding designed can potentially strengthen the films and even customize their mechanical performance (Zhang, Tao, Liu, & Wang, 2022). Previous research showed embedded patterns differing in materials and geometric configuration resulted in different mechanical properties of metal electrode films (K.-W. Lee, Lee, & Kim, 2020) and mesh/membrane composite structure (Zhang et al., 2022).

Conventionally, the aforementioned embedded pattern designs in films were achieved by using molding. Although molding provides high-quality, cost-effective pattern designs, it does not allow for quick customization. In recent years, 3D printing technology is therefore employed to customize structural designs in filling density and other dimensional properties (e.g. height) of objects to achieve different mechanical properties. It has, for instance, been used to maximize mechanical anisotropy of certain structures (e.g. for meat analogues, hydrogel scaffolds, and building materials) (Aldana, Valente, Dilley, & Doyle, 2021; Calton, Lille, & Sozer, 2023; Grabowska, Tekidou, Boom, & van der Goot, 2014; Torrado & Roberson, 2016). Mechanical anisotropy of printed objects can be induced either by printing pattern designs or by anisotropy of certain ink components themselves. Due to the high shear forces present in the nozzle, elongated fibers (e.g. cellulose fibers) have shown to align in the direction of extrusion (Sydney, Matsumoto, Nuzzo, Mahadevan, & Lewis, 2016). Recent studies have demonstrated the use of shear-induced alignment of anisotropic cellulose fibers in edible ink to enhance mechanical strength (e.g. tensile strength or Young's modulus) in the extrusion direction of 3D printed objects (Siqueira et al., 2017; Wang et al., 2018). However, the current study has rarely mentioned applying embedded pattern designs, reinforced with shear-induced alignment of fibers, to modify gelatin films.

Therefore, the aim of this study is to investigate the effects of embedded pattern designs (i.e. line, grid, and triangle) and edible ink compositions on mechanical properties of fish gelatin-based films. We hypothesized that printing embedded patterns in gelatin films could improve their mechanical properties and induce mechanical anisotropy. Furthermore, cellulose fibers (CF) as a plant fiber, is widely used in food products as a reinforcing agent, thickening agent, and low-calorie food filler. The CF is expected to increase the tensile strength of filaments in extrusion direction by 3D printing. Thus, the effect on film of shear-induced CF alignment is tested via the addition of CF in edible inks. Edible inks consisted of sodium caseinate (CA), sodium alginate (AL) and various concentrations of CF (0, 1.5, 3 and 6 g/100 mL). Gelatin films were fabricated by first 3D-printing the embedded pattern and then casting the gelatin film-forming solution over the pattern, after which the mixture was dried. The gelatin film-forming solution was fortified with  $\text{Ca}^{2+}$  ions to induce cross-linking with alginate. The mechanical performance of the films was determined by using tensile test. Cutoffs of films were stretched in different directions (i.e. parallel, perpendicular, and diagonal). The cross section of films is then investigated using Scanning Electron Microscopy (SEM), to better understand the fracture mechanics during stretching. Moreover, the shear-induced orientation of CF in the printed filaments was captured by using Confocal Laser Scanning Microscopy (CLSM).

## 2. Materials and methods

### 2.1. Materials

Sodium caseinate (CA, from bovine milk, containing 80 g/100 mL of the total protein in bovine milk, catalog number: C8654), sodium alginate (AL, catalog number: W201502), fish gelatin (from cold-water fish skin, molecular weight: 60 kDa, IEP:  $\sim$ 6.2, catalog number: G7041), cellulose fibers (CF, average length, 50  $\mu\text{m}$ , catalog number: C6288), calcium chloride ( $\text{CaCl}_2$ ), and glycerol were purchased from Sigma-Aldrich (Darmstadt, Germany). For all experiments deionized water was used.

### 2.2. Preparation of gelatin film-forming solution

The gelatin film-forming solution was prepared by dissolving fish gelatin (8 g/100 mL) and glycerol (4 g/100 mL) in deionized water and stirring at 60 °C for 2 h using a magnetic stirrer (C-MAG HS 7 digital; IKA, Staufen, Germany). After gradually cooling down to ambient temperature, the film-forming solution was then stirred with  $\text{CaCl}_2$  (1 g/100 mL) for 10 min, and stored at 4 °C for further use.

### 2.3. Preparation of printing materials

To totally dissolve sodium caseinate, a 15 g/100 mL sodium caseinate dispersion was made by incubating in a shaking water bath ((TW8, Julabo GmbH, Seelbach, Germany) at 100 rpm, 80 °C for 2 h. A 1.5 g/100 mL sodium alginate was added into the mixture and continued incubated for 2 h. After adding CF (0, 1.5, 3, and 6 g/100 mL), the samples were stirred for 6 h at 80 °C using a magnetic stirrer. To remove air bubbles from the solution, these formulations were transferred into centrifuge cups and centrifuged 10 min at a speed of 2000 rpm using a planetary vacuum centrifuge (Thinky Vacuum Mixer ARV-310LED, USA) with a pressure of 30 kPa, prior to every 3D printing experiment.

### 2.4. Determination of rheological properties

#### 2.4.1. Determination of gelation temperature

For the rheology experiments, an Anton Paar Physica MRC301 rheometer was used (Anton Paar GmbH, Graz, Austria). The gelation temperature of sodium caseinate-sodium alginate-CF (CA-AL-CF) inks was determined with a temperature ramp test (Schutyser, Houlder, de Wit, Buijsse, & Alting, 2018). After heating the inks at 80 °C for 15 min in a water bath, they were transferred to the preheated plate (60 °C), and excessive material was carefully removed. The parallel plate geometry (PP50-2, a 50 mm plate and plate geometry) was used, with a 0.497 mm gap. To prevent any evaporation of moisture during the measurement, paraffin oil was added around the edge of the sample. After loading the sample, it was equilibrated for 10 min, before starting the measurement. The strain and frequency for the temperature ramp test were set to 3% and 1 Hz, respectively. The temperature of the system was gradually decreased from 60 °C to 10 °C at a rate of 2.5 K/min, and then increased again from 10 °C to 60 °C at the same rate. The temperature, storage modulus ( $G'$ , Pa) and loss modulus ( $G''$ , Pa) of the system were recorded at a time interval of 1.5 s. The gelation temperature ( $T_{\text{gel}}$ , °C) was defined as the temperature at which the storage modulus  $G'$  exceeded that of the loss modulus  $G''$ .

#### 2.4.2. Determination of shear viscosity properties

The shear viscosity was measured using a parallel plate geometry (PP50-2, a 50 mm plate and plate geometry) over a shear rate range of 0.1–100/s (Zhang, Versteeg, Alting, & Schutyser, 2020). The test was performed at a temperature of 35 °C ( $T_p$ ), which was slightly above the measured  $T_{\text{gel}}$  (Liu, Bhandari, Prakash, Mantihal, & Zhang, 2019).

### 2.5. Printing the geometric structure

Three different geometric structures were designed using the open-source Slic3r 1.3.0 software (<https://slic3r.org/>), by varying the infill patterns with same extrusion value. For fair comparison between the different structures, the G-code was adjusted to make sure they had similar extrusion volumes, as determined by the software. This includes line (fill density 20.0%, printing volume 96.66  $\text{mm}^3$ , extrusion value 0.17 mm), grid (fill density 23.0%, printing volume 96.99  $\text{mm}^3$ , extrusion value 0.17 mm), and triangle patterns (fill density 21.8%, printing volume 96.08  $\text{mm}^3$ , extrusion value 0.17 mm) (Fig. 1A).

Printing was performed using an extrusion-based 3D food printer (Procusini 5.0, Germany), with a heated syringe. First, the printing ink,

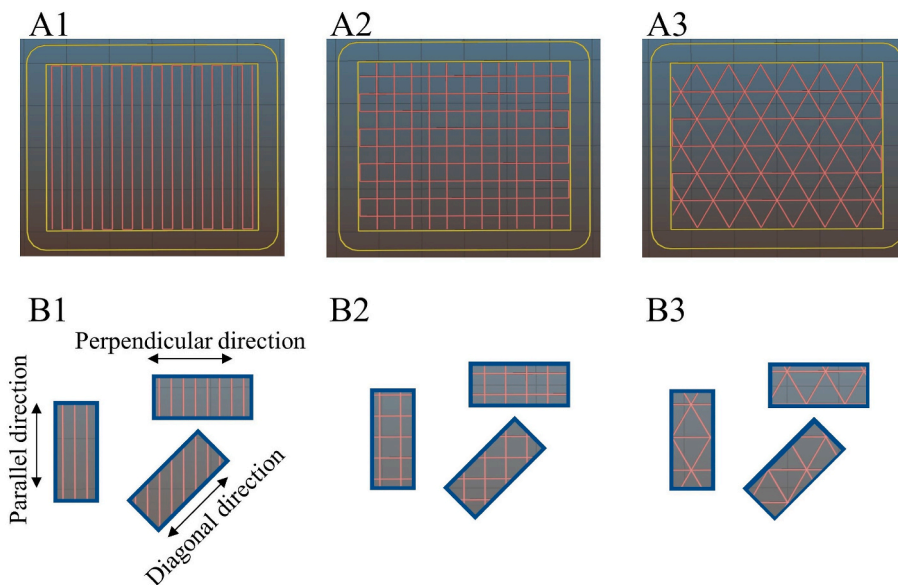


Fig. 1. The visual simulation geometric structure model (line, grid, and triangle), demo size (5 × 4 cm) (A1-A3); Schematic diagram of three stretching directions in different structure model (parallel, perpendicular and diagonal directions) (B1-B3).

vacuum centrifuged, was carefully transferred into a metal printing syringe ( $\varnothing = 27$  mm) with a tapered nozzle, having an outlet diameter of 0.41 mm (Optimum® SmoothFlow™ tapered dispensing tips, Nordson EFD). To ensure easy extrusion of all the inks, they were then incubated at 35 °C ( $T_p > T_{gel}$ ) in syringes, for 20 min prior to printing. The printing rate was kept constant at 10 mm/s and all printing designs based on the corresponding G-codes were used. Each printing pattern was printed into a Petri dish with an inner diameter of 9 cm.

## 2.6. Casting of gelatin film

The gelatin film-forming solution was casted on the plate containing the printed pattern, ensuring a final weight of 15.0 g, then dried at 40 °C  $\pm$  2 °C and 40%  $\pm$  2% relative humidity (RH) for 48 h in an environmental chamber (F.lli Della Marca, Italy). Pure gelatin film without printed pattern was control film. All films were peeled off and equilibrated at 23 °C  $\pm$  2 °C and 50%  $\pm$  8% RH for at least 72 h (Sun, Huang, Chen, Liu, & Leng, 2023).

## 2.7. Determining the film thickness and moisture content

The film thickness was determined using a digital caliper (Mitutoyo, Kawasaki, Japan); the average value of 10 random locations (center and perimeter) was determined for each film. The moisture content of the films was determined by recording the mass loss after drying small strips of film (2-cm in diameter) in a convection oven (Heraeus, Germany) at 105 °C for 24 h and calculated using Equation (1):

$$MC (\%) = \left( \frac{\Delta m}{m} \right) \times 100 \quad (1)$$

where,  $\Delta m$  is mass loss after drying (g) and  $m$  is the initial mass (g). Measurements were performed in five replicates.

## 2.8. Confocal scanning laser microscope

Confocal scanning laser microscope (CSLM) analysis was performed to visualize the alignment and location of CF in the different single filament samples. 250  $\mu$ L of Calcofluor white (0.1 g/L, excitation at 405 nm) was added into 50 ml CA-AL-CF inks and stirred for 2 min, before being centrifuged for 10 min at a speed of 2000 rpm. After the printing process, the filaments were transferred onto glass slides with grooves,

then covered with cover slips, to prevent the filament from being pressed and deformed. The images were made using a CSLM (Stellaris 5 Confocal LSM Leica, Germany) with a 20X lens under a scanning frequency of 100 Hz and pixel of 512 × 512, processed by using LAS X Office (Leica Microsystems, Germany) and ImageJ software (NIH, Bethesda, Maryland, USA). To calculate alignment of CF, the ImageJ plugin Directionality is used to infer the amount of CF in different orientations with computing a related histogram. A Gaussian fit is applied to the resulting histograms (Sydney et al., 2016).

## 2.9. Mechanical test

The tensile properties (tensile strength (TS) and elongation at break (EAB)) of the films were measured using a texture analyzer (Stable Micro System, Godalming, UK) following a previously described method with some modifications (Sun et al., 2023). The film samples were cut to 10 mm wide strips from three stretching directions using a knife (parallel, perpendicular, and diagonal to the printing directions, Fig. 1B). The film strips were stretched at a rate of 1 mm/s until the breaking point. TS (Pa) and EAB (%) were calculated using Equations (2) and (3):

$$TS (\text{Pa}) = F/A \quad (2)$$

$$EAB (\%) = \frac{\Delta L}{L_0} \times 100 \quad (3)$$

where,  $F$  is the maximum load (N) and  $A$  is the initial cross-sectional area of the specimen ( $\text{m}^2$ ).  $\Delta L$  is the change in the initial length up to the breaking point (m) and  $L_0$  is the initial length (m). Measurements were performed in six replicates.

To determine the mechanical anisotropy of the films, the anisotropy index (AI) was determined based on the ratio between the average value for the tensile strength measured in the parallel and perpendicular directions (Grabowska et al., 2014):

$$AI = \frac{TS_{\parallel}}{TS_{\perp}} \quad (4)$$

where  $TS_{\parallel}$  and  $TS_{\perp}$  represent the tensile strength (Pa) at parallel and perpendicular directions to the printed platform, respectively.

## 2.10. Scanning electron microscopy

The morphology of the cross-sections of the film specimens were performed before and after stretching. Unstretched films were put in liquid nitrogen and manually fractured without delay. The stretched films were collected after the tensile tests. The cross-sections of the stretched and unstretched specimens were coated with a thin layer of gold using a JEOL Smart-Coater (JEOL, Japan) and were subsequently analyzed using scanning electron microscopy (SEM, JEOL JCM-7000) at an accelerating voltage of 5 kV.

## 3. Results and discussion

### 3.1. Rheological characterization and printing performance

For the successful flow of filaments from the nozzle, the temperature of the cartridge needs to be adjusted based on the gelation temperature of the different inks. The gelation temperature of sodium caseinate-sodium alginate without CF was 11.44 °C, while for adding CF of 1.5 g/100 mL, 3 g/100 mL, and 6 g/100 mL, the gelation temperature was increased to 25.02 °C, 24.28 °C, and 29.91 °C (Fig. 2). Having a gelation temperature above room temperature means that the printing cartridge needs to be heated for printing, and the filaments solidify under on the printing platform without the need for cooling. The results are in line with our previous study, where sodium caseinate systems did not gel at room temperature at low concentrations (protein  $\leq$  15 g/100 mL) (Schutyser et al., 2018). The clear improvement of gelation temperature with increasing concentration of CF could be explained by the interactions of caseinate to CF (Xiao et al., 2020). The rheological behaviors of protein/cellulose fibers were improved by strong intra- and intermolecular interactions of protein molecules and cellulose chains. The shear viscosity and shear stress profiles of CA-AL-CF inks at different concentration are shown in Table 1. All inks exhibited typical shear thinning behavior at 35 °C ( $T_p > T_{gel}$ ) associated with biopolymer dispersions (Smith, Basu, Saha, & Nelson, 2018). The disruption of intermolecular forces in biopolymers at high shear rates is the major cause of shear thinning. The viscosity increased with increasing CF concentration, similar to the gelation temperature. In addition to the increase intermolecular forces between CF and sodium caseinate-sodium alginate, the CF has an elongated, rod-like shape that could increase the viscosity of the ink (Xiao et al., 2020).

The printability of the different inks is assessed by evaluating the filament width after printing. These widths of filaments showed some variation (790~1020  $\mu$ m, Table 1) but were all larger than the diameter

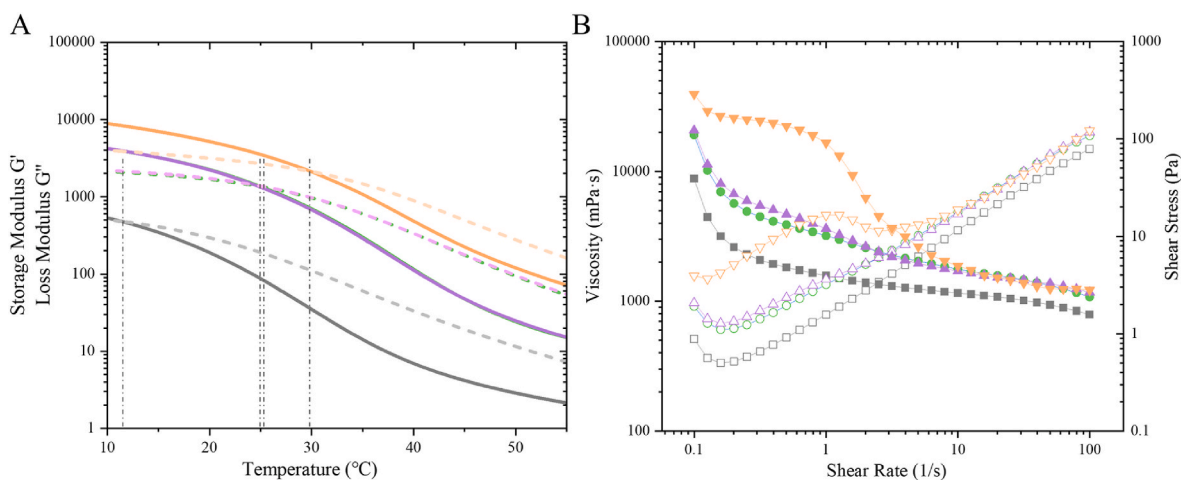
of printing nozzle (410  $\mu$ m). This increase in width is expected to be due to die swell, also called the Barus effect, previously observed in similar systems (Ma et al., 2023). Normal stress differences in a just extruded ink between the wall pressure and the atmospheric pressure cause the filament to expand after ejection (Hori & Okubo, 1980; Wang et al., 2021). The width of filaments was significantly different apart from those containing 6 g/100 mL CF, which were thinner (Table 1). This difference might be related to fact that 6 g/100 mL CF had a  $T_{gel}$  that was just below the printing temperature, ensuring quicker gelation after deposition. In addition, the higher ink with 6 g/100 mL CF had a higher viscosity, which leads to less spread and thus thinner filaments (Wang et al., 2021).

When the printing temperature is chosen adequately, the gelation process is quick after deposition, leading to little diffusion of filaments and cross points. There is no significant change in thickness of all film and in moisture content of different structure films. In the case of 6 g/100 mL CF, not only was the filament width smaller, it also had relatively bigger hole areas of corresponding structures, with higher shape fidelity. However, some patterns did show the under-extrusion, especially for the line structure. This under-extrusion is possibly due to the clogging of the nozzle or limitations of the nozzle type (Ma, Schutyser, Boom, & Zhang, 2022). Wider filaments indicate more spreading after deposition, and thus less hole areas of corresponding structures. The lower fidelity of structures printed with other concentrations also could be explained by their gelation temperature close or lower to room temperature, leading to over extrusion at the start, stop or cross points and rounding off of the printed shape. Note that the focus of this work is on the effect of different printing patterns, which are subject to the same printing performance (per ink). In future studies the printing accuracy could be improved by adjusting the printing temperature to the individual gelation temperature and/or the printing settings to the rheological behavior, which would further improve comparison. This is, however, considered to be out of scope for this study.

### 3.2. Mechanical performance of films

#### 3.2.1. Mechanical properties of line structure


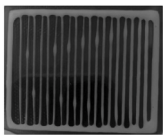
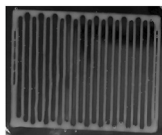
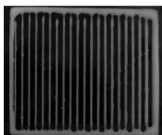
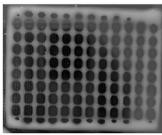
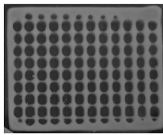
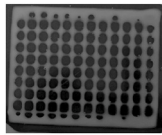
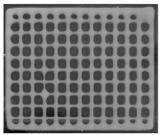
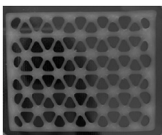
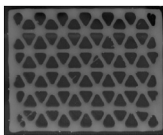
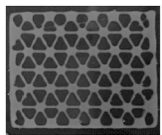
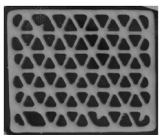
Generally, a uniform film can be obtained using ordinary casting methods. Inside these films there is no directional dependence, which means that the mechanical properties are the same in all directions (Sydney et al., 2016). This was confirmed by adding components with the same concentration as the filaments to the film-forming solution and using the casting method to produce blended films. The resulting films showed no directional dependence and no significant difference in



**Fig. 2.** Gelation temperature ( $T_{gel}$ ) of different concentration of CA-AL-CF ink (A); Viscosity and shear stress profiles for different concentration of CA-AL-CF ink at temperature of 35 °C ( $T_p$ ) (B). Solid lines show the storage modulus  $G'$  and dotted line show the loss modulus  $G''$ . Closed symbols show the viscosity (mPa·s) and open symbols show the shear stress (Pa). Grey, green, purple, and orange represent CA-AL-0CF, CA-AL-1.5CF, CA-AL-3CF, and CA-AL-6CF, respectively.

**Table 1**

Printing performance of different structures including thickness of film, actual printed pattern, and hole area of corresponding structures; Filament widths with different concentration of CF.

Structure	Concentration of CF (%w/v)	0	1.5	3	6
Line	Thickness of film (mm)	0.30 ± 0.03 <sup>a</sup>	0.30 ± 0.03 <sup>a</sup>	0.26 ± 0.02 <sup>a</sup>	0.26 ± 0.05 <sup>a</sup>
	Printed pattern				
Grid	Hole area (mm <sup>2</sup> )	10.02 ± 2.59 <sup>b</sup>	12.50 ± 0.55 <sup>b</sup>	11.24 ± 1.92 <sup>b</sup>	15.06 ± 0.01 <sup>a</sup>
	Thickness of film	0.30 ± 0.02 <sup>a</sup>	0.28 ± 0.03 <sup>a</sup>	0.25 ± 0.03 <sup>a</sup>	0.24 ± 0.05 <sup>a</sup>
Triangle	Printed pattern				
	Hole area (mm <sup>2</sup> )	7.55 ± 0.74 <sup>b</sup>	10.03 ± 1.05 <sup>a</sup>	9.17 ± 0.91 <sup>a</sup>	10.54 ± 0.58 <sup>a</sup>
Triangle	Thickness of film	0.28 ± 0.02 <sup>a</sup>	0.26 ± 0.03 <sup>a</sup>	0.28 ± 0.03 <sup>a</sup>	0.26 ± 0.04 <sup>a</sup>
	Printed pattern				
Width of filament (mm)	Hole area (mm <sup>2</sup> )	11.37 ± 0.37 <sup>b</sup>	10.78 ± 0.36 <sup>b</sup>	10.25 ± 1.49 <sup>b</sup>	13.40 ± 1.49 <sup>a</sup>
	Thickness of film	1.03 ± 0.027 <sup>b</sup>	0.91 ± 0.240 <sup>ab</sup>	1.02 ± 0.060 <sup>b</sup>	0.74 ± 0.180 <sup>a</sup>

Different letters within the same row indicate a significant difference ( $p < 0.05$ ). Thickness of pure gelatin film was  $0.29 \pm 0.08$  mm.

mechanical strength compared to pure gelatin films (Fig. S1). The directional dependence and tensile strength did change when the reinforced film was made using the printed embedded structures (Fig. 3). For instance, the tensile strength of films with a line-structure reinforcement significantly increased compared to pure gelatin films, in the parallel and diagonal directions (Fig. 3A). Only in the perpendicular direction, the tensile strength was shown to decrease. As expected, samples stretched in the parallel direction had highest tensile strength, being in the direction of the line structure. This result indicated that using 3D printing to concentrate components as a structural backbone to resist external forces is clearly effective. It also shows a positive correlation with concentration of CF, because filler characteristic of CF was also contributed enhancement of filaments (Gutiérrez & Alvarez, 2017). For the elongation at break (EAB), an opposite trend was observed (Fig. 3B). The EAB in the perpendicular direction is significantly larger than in other directions. It is precisely because of the reinforcement in the parallel direction that the extension is limited. Due to the interference of the filaments with the cross-linking between gelatin, as well as the change in the distribution of glycerol, the extension in the vertical direction is lower than that of the pure gelatin film. These results indicated that stretching orientation played a major role on both tensile strength and elongation, similar to the study of Allum, Gleadall, and Silberschmidt (2020). To further improve the mechanical properties and reduce the limitation of elongation at break, it is possible to consider adjusting the proportion of glycerol in the future. Focus on specimens with line structure themselves, stretching direction and concentration of CF also had a significant interaction effect between them ( $F(6, 18) = 3.28, p = 0.023$ ).

### 3.2.2. Mechanical properties of grid and triangle structures

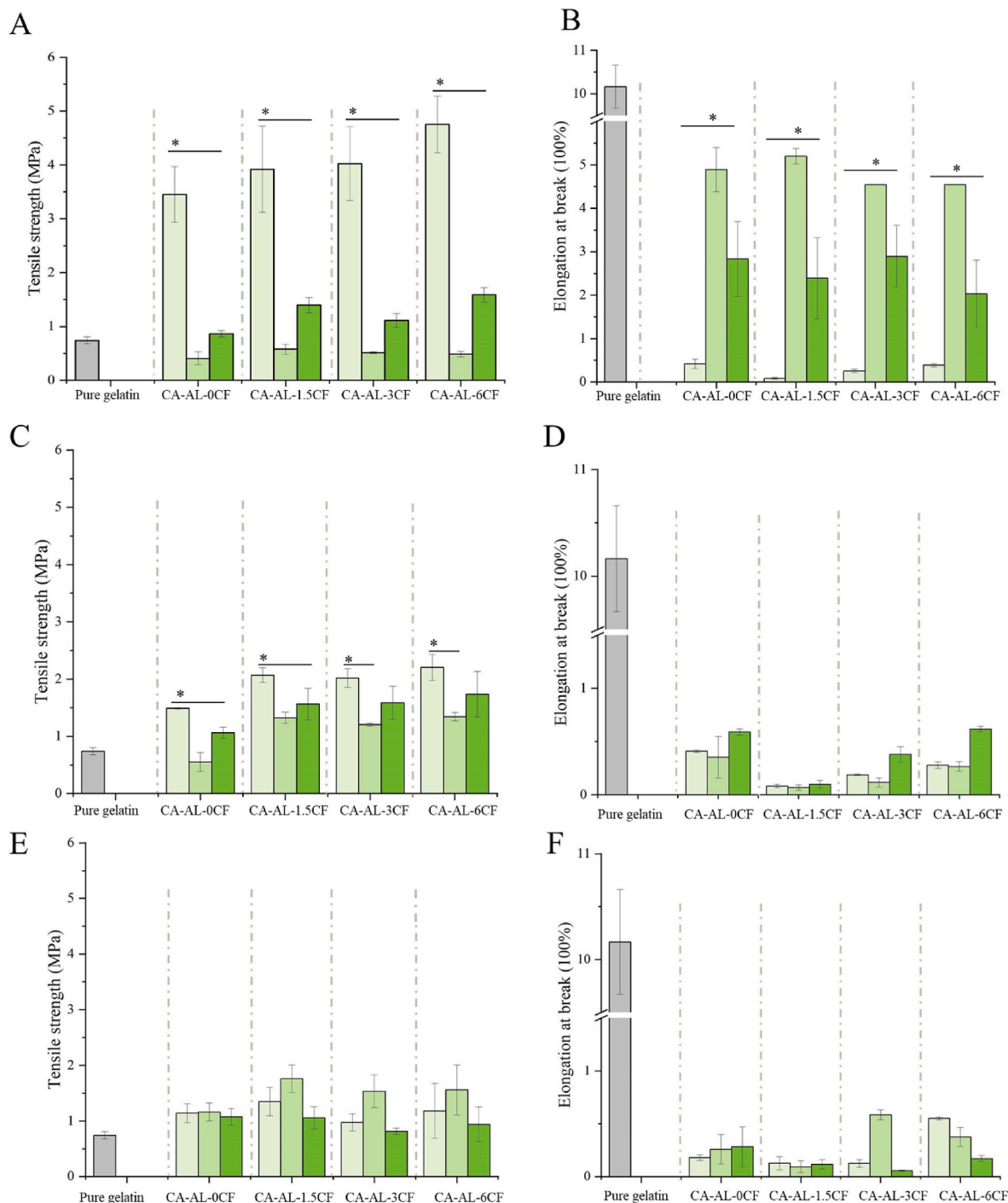
In other structures, due to the overlapping of lines and complexity of design geometric pattern, composite films with grid and triangle patterns exhibited different tensile resistance in different stretching directions. For the grid structure (Fig. 3C–D), stretching direction had a significant effect on the tensile strength ( $F(2, 21) = 23.35, p < 0.01$ ). The tensile strength was the largest in the parallel direction ( $p < 0.05$ ).

For double-layer or multilayer geometric structures, the printing sequence significantly influences their resistance to stretching forces from different directions. The grid, for instance, is composed of two layers. The first layer is printed in the parallel direction, and the second layer is printed in the perpendicular direction. During printing of the second layer, some materials converged into cross point reducing the second layer dosage in between crosspoints. This leads to a quicker rupture of filaments when stretched in the printing direction of the second layer. In addition, the printing sequence due to the difference time of exposure to room temperature also affected the width of layer. Vanaei et al. (2020) observed that the filaments were deformed with the cumulation of layers due to temperature evolution, leading to a different force distribution in the overall structure. Therefore, the grid structure in this printing sequence achieved maximum TS in the parallel direction (Supporting V1). The opposite was observed when the printing sequence was changed, i.e. first in the perpendicular direction and then in then parallel direction. Results are presented in Fig. S2 and Supporting V2.

The triangle structure is made up of angular lines (Fig. 1). These filaments are more easily deformed by applied forces, acting similarly to a cantilever beam (Cabreira & Santana, 2020). A high tensile strength is only observed when one of the triangular filaments is parallel to the stretching forces, e.g. when stretching in the perpendicular direction. As the embedded structure interrupts the continuous gelatin film in more directions, it makes the film more prone to rupture, leading to a lower TS. Therefore, the stretching direction had a significant effect on the TS of the triangle structure ( $F(2, 17) = 14.32, p < 0.01$ ) (Fig. 3E–F).

### 3.2.3. Anisotropic index

An anisotropy index quantifies how directionally dependent the properties are of a structure (Kube, 2016). For the tensile stress, the anisotropy index of the composite film with triangle structure was approximately 1, indicating no directional dependency (Fig. 4). In the case of line and grid structures, the anisotropy index was higher than 1. With the same printing ink dosage, it is thus possible to induce anisotropy with respect to TS. As expected, the line structure has the highest anisotropy index in terms of TS, with a maximum anisotropy index of



**Fig. 3.** Tensile strength (TS) of line structure in different direction (A). Elongation at break (EAB) of line structure in different direction (B). TS of grid structure in different direction (C). EAB of grid structure in different direction (D). TS of triangle structure in different direction (E). EAB of triangle structure in different direction (F). \* Indicates statistical significance at  $p < 0.05$ . ■ represent parallel stretching direction, ■ represent perpendicular stretching direction, ■ represent diagonal stretching direction.

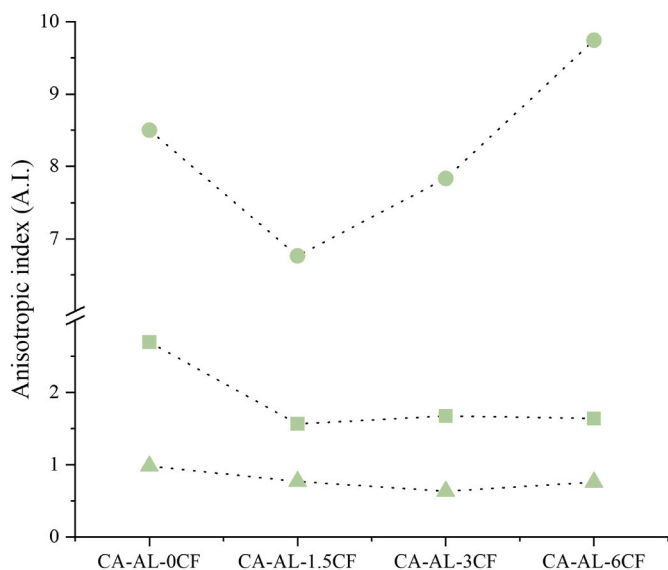
9.75 in the case of CA-AL-6CF. The filaments in the parallel direction of the line structure utilize all printing material dosage, whereas the printing material dosage for grid or triangle structures is dispersed in the two or three directions, resulting in less pronounced anisotropy.

The difference in tensile strength and anisotropy index shows that reinforcing the internal structure of the film with simple geometric structure can lead to changes in its mechanical properties. This is more effective compared to simply blending the same printing materials into the film (Fig. S1). While a line structure may offer more effective in

enhancing mechanical properties, it's crucial to know that difference in geometric structures could fulfill different application purposes. This could, for instance, be for packages that require tearing (Lee, Register, & Dean, 2005).

### 3.3. Fracture mechanics

By observing the fracture surface of the specimen using SEM it is possible to indirectly analyze the specimen's ability to resist external



**Fig. 4.** Results for the anisotropic index in TS of composite film with different structure. Circle, square, and triangle symbols represent line, grid, and triangle printing structures, respectively.

forces and get insights into the fracture mechanism (Fu, Li, Hu, Hu, & Nie, 2020). In case of unstretched films, the cross section is obtained after freezing in liquid nitrogen and manually breaking the film, causing rapid fracture (Fig. 5A1-5A5). In Fig. 5A, the cross section of pure gelatin film was smooth and homogeneous. In composite films, the filament is visible due to its difference in density compared to the rest of the gelatin film. Fig. 5B1-5B5 show the specimens underwent transverse fracture after applying a stretching force. The cross section of the pure gelatin film kept smooth, whereas the cross section of filaments in composite films was observed to become rough and form an irregular cavity structure. This suggests that the filament endured most of the forces on the composite film, as the difference in the fracture surfaces has been linked to a greater toughness of filament parts (Dear, 1999). This is also supported by the higher tensile strength (Fig. 3) and is in agreement with the studies performed by Ayatollahi, Nabavi-Kivi, Bahrami, Yahya, and Khosravani (2020). They revealed that the irregular markings in fracture surfaces of poly-lactic acid dog-bone specimens increased with increasing area under the stress-strain curve. These results demonstrated that the damage area and irregularity of the fracture surface are

positively correlated with energy dissipation, which also reflects in the tensile strength of the material. The roughness of the fracture surface did not appear to have a significant relationship with concentration of CF.

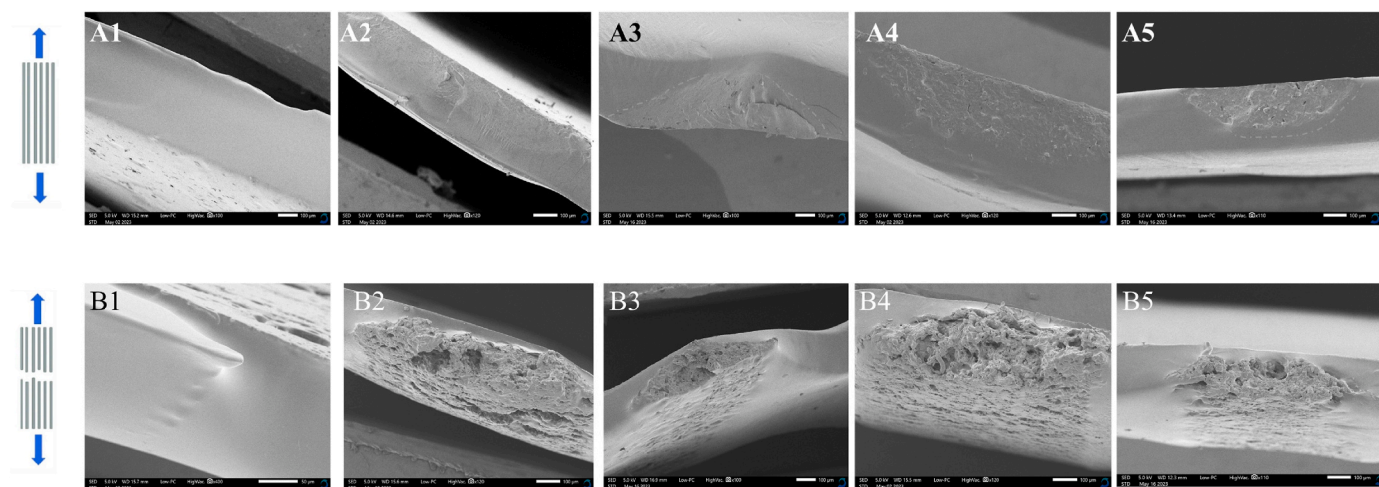
### 3.4. Alignment of cellulose fibers

In order to investigate the relationship between extrusion direction and orientation of CF after printing, CLSM was used. After staining with Calcofluor white, the distribution of CF in different inks can be observed (Fig. 6A-E). As control, a sample without CF is included (Fig. 6D). The control shows several oval droplets, representing the phase separation of sodium caseinate and alginate in the filament. This indicates that simple blending of sodium caseinate and alginate can't produce fibrous structures, but requires fixation inside a calcium loaded agar gel, as shown by Zhu, Wang, Stieger, van der Goot, and Schutyser (2022). As shown by the yellow arrows, CF in the cast sample without printing had a random distribution without directionality (Fig. 6E), indicated that the casting process did not induce anisotropy. In the printed samples, significant CF alignment is directly observed. During the extrusion process, as the cross-section area of the deposition nozzle decreases, the flow velocity of the ink increases. The CF undergoes shear-induced alignment along with the direction of ink flow. This results in printed filament exhibiting anisotropic stiffness (Håkansson et al., 2014).

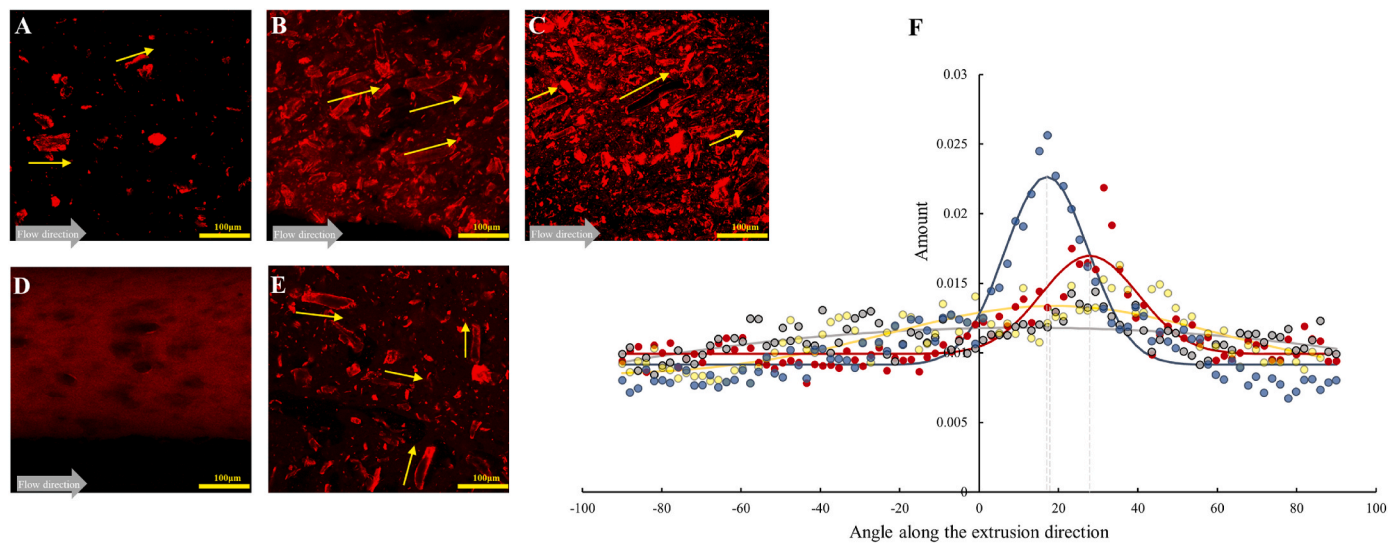
The directionality of the fibers in the cast sample and printed filaments is quantified by Fourier analysis confocal images. The printed filaments had relatively clear directionality peaks, whereas this was not the case for the casting sample (Fig. 6F). Among them, the printed filament with 3 g/100 mL CF had the most obvious quantitative directionality, which might be because excessively high concentrations (6 g/100 mL) hinder the motion of CF arranged toward the extrusion direction. The above results proved that the CF aligns itself during the printing process, and this alignment to the printing direction provides anisotropy to the filament and thereby affects the resistance to external forces. Overall, alignment of CF could contribute to the change mechanical properties of filament. In designing structures, optimization can be achieved by adjusting the concentration of CF, but as shown in Section 3.2, the structural design still dominates mechanical properties.

## 4. Conclusions

Edible biopolymers are increasingly used in commercial food products as sustainable packaging materials. For this, cold-water fish gelatin could be an interesting alternative, as it is a by-product of fish processing. However, films made of fish gelatin show poor mechanical



**Fig. 5.** A-B: The cross-section images of pure gelatin film and composite films with line structure before (A1-A5) and after fracture (B1-B5). Pure gelatin film was used as the control (A1 & B1), Number 2 to 5 indicates prints using inks with different CF concentrations (0, 1.5, 3 and 6 g/100 mL).



**Fig. 6.** A–E: Confocal images of Calcofluor White stained samples by CLSM, A: Printed of CA-AL-1.5CF sample, B: Printed of CA AL-3CF sample, C: Printed of CA-AL-6CF sample, D: Printed of CA-AL-0CF sample, E: Casting of CA-AL-3CF sample; F: Quantification directionality analysis of confocal images for casting and printed filament with CF. The yellow arrow represents direction of CF. The grey arrow represents printed direction of filament. Circle symbols represent the measured values of CF orientation distributions and solid lines represent fitted curve of CF orientation distributions. Grey, yellow, blue, and red represent casting of CA-AL-3CF sample, printed of CA-AL-1.5CF sample, printed of CA AL-3CF sample, and printed of CA-AL-6CF sample, respectively.

properties. We investigated if these mechanical properties could be improved by printing embedded patterns to support the gelatin films and by adding cellulose fibers to the support structure. Gelatin films with embedded line, grid and triangle structures were compared to plain gelatin films with the same total biopolymer content. At the same ink dosage, an embedded line structure provided the maximum anisotropy index and tensile strength in the parallel stretching direction, followed by the grid and triangle structures. For all reinforced films, the elongation at break was reduced. In the case of structures with two layers, i.e. with the cross-over point of grid structures, the tensile strength is lower when the film is stretched in the direction of the second layer. This shows that optimization of the printing path is possible. The addition of cellulose fibers in sodium caseinate-sodium alginate ink system increased the gelation temperature, and also enhanced the resistance of filament through alignment in the extrusion direction. The alignment of cellulose fibers requires further investigation by adjusting parameters, such as fiber size, type, and proportion in the embedded patterns. This study confirmed that structural design and printing materials with anisotropic properties have the ability to improve the mechanical strength of cold-water fish gelatin films. These improvements could provide practical use in applications such as easy tearing packaging that are reinforced only in one direction. Our findings provide a step forward towards the use of cold-water fish gelation as sustainable packaging material.

#### CRediT authorship contribution statement

**Hongbo Sun:** Writing – review & editing, Writing – original draft, Validation, Methodology, Investigation, Formal analysis, Conceptualization. **Xiaoqing Leng:** Funding acquisition. **Xiaonan Sui:** Conceptualization. **Lu Zhang:** Writing – review & editing, Supervision, Conceptualization. **Patrick Wilms:** Writing – review & editing, Validation, Supervision, Conceptualization.

#### Declaration of competing interest

The authors declare that they have no known competing financial interests or personal relationships that could have appeared to influence the work reported in this paper.

#### Data availability

Data will be made available on request.

#### Acknowledgements

Special thanks to Yizhou Ma for his help with setting-up the 3D printer, Jarno Gieteling and Maurice Strubel for making image analysis techniques, Jos Sewalt for making the rheology analysis techniques. The authors acknowledge support received from the China scholarship council (202206350013) for supporting this work. Lu Zhang would also like to acknowledge the financial support from NWO Sectorplan Mechanical Engineering on Additive Food Assembly research at the Laboratory of Food Process Engineering, Wageningen University & Research.

#### Appendix A. Supplementary data

Supplementary data to this article can be found online at <https://doi.org/10.1016/j.lwt.2024.116839>.

#### References

- Aldana, A. A., Valente, F., Dilley, R., & Doyle, B. (2021). Development of 3D bioprinted GelMA-alginate hydrogels with tunable mechanical properties. *Bioprinting*, *21*, Article e00105. <https://doi.org/10.1016/j.bprint.2020.e00105>
- Allum, J., Gleadall, A., & Silberschmidt, V. V. (2020). Fracture of 3D-printed micro-tensile specimens: Filament-scale geometry-induced anisotropy. *Procedia Structural Integrity*, *28*, 591–601. <https://doi.org/10.1016/j.prostr.2020.10.069>
- Ayatollahi, M. R., Nabavi-Kivi, A., Bahrami, B., Yazid Y, M., & Khosravani, M. R. (2020). The influence of in-plane raster angle on tensile and fracture strengths of 3D-printed PLA specimens. *Engineering Fracture Mechanics*, *237*, Article 107225. <https://doi.org/10.1016/j.engfracmech.2020.107225>
- Cabreira, V., & Santana, R. M. C. (2020). Effect of infill pattern in fused filament fabrication (FFF) 3D printing on materials performance. *Matéria. Revista Internacional d'Art*, *25*(3). <https://doi.org/10.1590/S1517-707620200003.1126>
- Calton, A., Lille, M., & Sozer, N. (2023). 3-D printed meat alternatives based on pea and single cell proteins and hydrocolloids: Effect of paste formulation on process-induced fibre alignment and structural and textural properties. *Food Research International*, *174*, Article 113633. <https://doi.org/10.1016/j.foodres.2023.113633>
- Chen, J., Luo, L., Cen, C., Liu, Y., Li, H., & Wang, Y. (2022). The nano antibacterial composite film carboxymethyl chitosan/gelatin/nano ZnO improves the mechanical strength of food packaging. *International Journal of Biological Macromolecules*, *220*, 462–471. <https://doi.org/10.1016/j.ijbiomac.2022.08.005>



- Dear, D. J. P. (1999). A study of polymer fracture surface features and their relationship to toughness. *Journal of Materials Science*, 34(20), 4897–4907. <https://doi.org/10.1023/A:1004726702286>
- Fu, Y., Li, Y., Hu, A., Hu, H., & Nie, X. (2020). Microstructure, tensile properties and fracture behavior of squeeze-cast Mg alloy AZ91 with thick cross section. *Journal of Materials Engineering and Performance*, 29(6), 4130–4141. <https://doi.org/10.1007/s11665-020-04910-x>
- Ghosh, V., Ziegler, G. R., & Anantheswaran, R. C. (2005). Moisture migration through chocolate-flavored confectionery coatings. *Journal of Food Engineering*, 66(2), 177–186. <https://doi.org/10.1016/j.jfoodeng.2004.03.012>
- Grabowska, K. J., Tekidou, S., Boom, R. M., & van der Goot, A.-J. (2014). Shear structuring as a new method to make anisotropic structures from soy–gluten blends. *Food Research International*, 64, 743–751. <https://doi.org/10.1016/j.foodres.2014.08.010>
- Groh, K. J., Backhaus, T., Carney-Almroth, B., Geueke, B., Inostroza, P. A., Lennquist, A., et al. (2019). Overview of known plastic packaging-associated chemicals and their hazards. *Science of the Total Environment*, 651, 3253–3268. <https://doi.org/10.1016/j.scitotenv.2018.10.015>
- Gutiérrez, T. J., & Alvarez, V. A. (2017). Cellulosic materials as natural fillers in starch-containing matrix-based films: A review. *Polymer Bulletin*, 74, 2401–2430. <https://doi.org/10.1007/s00289-016-1814-0>
- Håkansson, K. M. O., Fall, A. B., Lundell, F., Yu, S., Krywka, C., Roth, S. V., et al. (2014). Hydrodynamic alignment and assembly of nanofibrils resulting in strong cellulose filaments. *Nature Communications*, 5(1), 4018. <https://doi.org/10.1038/ncomms5018>
- Hanani, Z. A. N., Yee, F. C., & Nor-Khaizura, M. A. R. (2019). Effect of pomegranate (*Punica granatum* L.) peel powder on the antioxidant and antimicrobial properties of fish gelatin films as active packaging. *Food Hydrocolloids*, 89, 253–259. <https://doi.org/10.1016/j.foodhyd.2018.10.007>
- Hernández, O., Emaldi, U., & Tovar, J. (2008). In vitro digestibility of edible films from various starch sources. *Carbohydrate Polymers*, 71(4), 648–655. <https://doi.org/10.1016/j.carbpol.2007.07.016>
- Hori, Y., & Okubo, S. (1980). On the normal stress effect and the Barus effect of polymer melts. *Journal of Rheology*, 24(1), 39–53. <https://doi.org/10.1122/1.549555>
- Hosseini, S. F., Javidi, Z., & Rezaei, M. (2016). Efficient gas barrier properties of multi-layer films based on poly(lactic acid) and fish gelatin. *International Journal of Biological Macromolecules*, 92, 1205–1214. <https://doi.org/10.1016/j.ijbiomac.2016.08.034>
- Kube, C. M. (2016). Elastic anisotropy of crystals. *AIP Advances*, 6, Article 095209. <https://doi.org/10.1063/1.4962996>
- Lee, K.-W., Lee, H.-J., & Kim, J.-Y. (2020). Fabrication and patterning of stretchable Ag nanowire network films embedded in an elastomeric polymer matrix. *Synthetic Metals*, 262, Article 116333. <https://doi.org/10.1016/j.synthmet.2020.116333>
- Lee, L.-B. W., Register, R. A., & Dean, D. M. (2005). Tear anisotropy in films blown from polyethylenes of different macromolecular architectures. *Journal of Polymer Science Part B: Polymer Physics*, 43(4), 413–420. <https://doi.org/10.1002/polb.20350>
- Li, M., Guo, L., Mu, Y., Huang, X., Jin, L., Xu, Q., et al. (2024). Gelatin films reinforced by tannin-nanocellulose microgel with improved mechanical and barrier properties for sustainable active food packaging. *Food Hydrocolloids*, 149, Article 109642. <https://doi.org/10.1016/j.foodhyd.2023.109642>
- Liu, Z., Bhandari, B., Prakash, S., Mantihal, S., & Zhang, M. (2019). Linking rheology and printability of a multicomponent gel system of carrageenan-xanthan-starch in extrusion based additive manufacturing. *Food Hydrocolloids*, 87, 413–424. <https://doi.org/10.1016/j.foodhyd.2018.08.026>
- Ma, Y., Potappel, J., Chauhan, A., Schutyser, M. A. I., Boom, R. M., & Zhang, L. (2023). Improving 3D food printing performance using computer vision and feedforward nozzle motion control. *Journal of Food Engineering*, 339, Article 111277. <https://doi.org/10.1016/j.jfoodeng.2022.111277>
- Ma, Y., Schutyser, M. A. I., Boom, R. M., & Zhang, L. (2022). Thermographic and rheological characterization of viscoelastic materials for hot-extrusion 3D food printing. *Innovative Food Science & Emerging Technologies*, 81, Article 103135. <https://doi.org/10.1016/j.ifset.2022.103135>
- Mohamed, S. A. A., El-Sakhawy, M., & El-Sakhawy, M. A.-M. (2020). Polysaccharides, protein and lipid -based natural edible films in food packaging: A review. *Carbohydrate Polymers*, 238, Article 116178. <https://doi.org/10.1016/j.carbpol.2020.116178>
- Ong, H.-T., Samsudin, H., & Soto-Valdez, H. (2022). Migration of endocrine-disrupting chemicals into food from plastic packaging materials: An overview of chemical risk assessment, techniques to monitor migration, and international regulations. *Critical Reviews in Food Science and Nutrition*, 62(4), 957–979. <https://doi.org/10.1080/10408398.2020.1830747>
- Schutyser, M. A. I., Houlder, S., de Wit, M., Buijsse, C. A. P., & Alting, A. C. (2018). Fused deposition modelling of sodium caseinate dispersions. *Journal of Food Engineering*, 220, 49–55. <https://doi.org/10.1016/j.jfoodeng.2017.02.004>
- Siqueira, G., Kokkinis, D., Libanori, R., Hausmann, M. K., Gladman, A. S., Neels, A., et al. (2017). Cellulose nanocrystal inks for 3D printing of textured cellular architectures. *Advanced Functional Materials*, 27(12), Article 1604619. <https://doi.org/10.1002/adfm.201604619>
- Smith, P. T., Basu, A., Saha, A., & Nelson, A. (2018). Chemical modification and printability of shear-thinning hydrogel inks for direct-write 3D printing. *Polymer*, 152, 42–50. <https://doi.org/10.1016/j.polymer.2018.01.070>
- Sun, H., Huang, Y., Chen, Y., Liu, X., & Leng, X. (2023). Effects of curcumin, phycocyanin, or modified lycopene colorants on the physicochemical and sensory properties of whey protein–cellulose nanocrystal packaging films. *Food Chemistry*, 412, Article 135541. <https://doi.org/10.1016/j.foodchem.2023.135541>
- Sydney Gladman, A., Matsumoto, E. A., Nuzzo, R. G., Mahadevan, L., & Lewis, J. A. (2016). Biomimetic 4D printing. *Nature Materials*, 15(4), 413–418. <https://doi.org/10.1038/nmat4544>
- Torrado, A. R., & Roberson, D. A. (2016). Failure analysis and anisotropy evaluation of 3D-printed tensile test specimens of different geometries and print raster patterns. *Journal of Failure Analysis and Prevention*, 16(1), 154–164. <https://doi.org/10.1007/s11668-016-0067-4>
- Vanaei, H. R., Raissi, K., Deligant, M., Shirinbayan, M., Fitoussi, J., Khelladi, S., et al. (2020). Toward the understanding of temperature effect on bonding strength, dimensions and geometry of 3D-printed parts. *Journal of Materials Science*, 55(29), 14677–14689. <https://doi.org/10.1007/s10853-020-05057-9>
- Wang, J., Liu, Y., Zhang, X., Rahman, S. E., Su, S., Wei, J., et al. (2021). 3D printed agar/calcium alginate hydrogels with high shape fidelity and tailor-made mechanical properties. *Polymer*, 214, Article 123238. <https://doi.org/10.1016/j.polymer.2020.123238>
- Wang, Q., Sun, J., Yao, Q., Ji, C., Liu, J., & Zhu, Q. (2018). 3D printing with cellulose materials. *Cellulose*, 25(8), 4275–4301. <https://doi.org/10.1007/s10570-018-1888-y>
- Xiao, Y., Liu, Y., Wang, Y., Jin, Y., Guo, X., Liu, Y., et al. (2020). Heat-induced whey protein isolate gels improved by cellulose nanocrystals: Gelling properties and microstructure. *Carbohydrate Polymers*, 231, Article 115749. <https://doi.org/10.1016/j.carbpol.2019.115749>
- Yang, Z., Chaieb, S., & Hemar, Y. (2021). Gelatin-based nanocomposites: A review. *Polymer Reviews*, 61(4), 765–813. <https://doi.org/10.1080/15583724.2021.1897995>
- Zhang, T., Sun, R., Ding, M., Li, L., Tao, N., Wang, X., et al. (2020). Commercial cold-water fish skin gelatin and bovine bone gelatin: Structural, functional, and emulsion stability differences. *Lebensmittel-Wissenschaft & Technologie*, 125, Article 109207. <https://doi.org/10.1016/j.lwt.2020.109207>
- Zhang, Y., Tao, Q., Liu, Y., & Wang, C. (2022). Mesh/membrane composite with superior mechanical performance: A deep learning-based design. *Composites Science and Technology*, 230(109735). <https://doi.org/10.1016/j.compscitech.2022.109735>
- Zhang, L., Versteeg, S., Alting, A. C., & Schutyser, M. A. I. (2020). Impact of conjugation with maltodextrin on rheological properties of sodium caseinate. *International Dairy Journal*, 105, Article 104660. <https://doi.org/10.1016/j.idairyj.2020.104660>
- Zhu, S., Wang, W., Stieger, M., van der Goot, A. J., & Schutyser, M. A. I. (2022). Shear-induced structuring of phase-separated sodium caseinate - sodium alginate blends using extrusion-based 3D printing: Creation of anisotropic aligned micron-size fibrous structures and macroscale filament bundles. *Innovative Food Science & Emerging Technologies*, 81, Article 103146. <https://doi.org/10.1016/j.ifset.2022.103146>